Forsch Ingenieurwes (2023) 87:39–50
https://doi.org/10.1007/s10010-023-00616-3

ORIGINALARBEITEN/ORIGINALS

Multi-domain optimization of cast iron components in wind turbines

Felix Weber[1] · Christoph Broeckmann[1] · Vitali Züch[2] · Georg Jacobs[2] · Jannik Zimmermann[3] · Kai-Uwe Schröder[3] · Youness Bami[4] · Jürgen Jakumeit[4] · Mathias Bodenburg[5] · Reinhard Weiß[6]

Received: 2 November 2022 / Accepted: 11 January 2023 / Published online: 20 March 2023

Abstract

The continuously rising demand for renewable energies leads to increased installations of wind turbines with higher power. While the current power-to-weight ratio of up to 20 metric tons of cast iron per megawatt is stagnating, cast iron components of modern wind turbines are facing new challenges in terms of weight, manufacturability, and castability. These challenges can be addressed by systematically using multi-domain optimization approaches to reduce component weight and increase local component utilization.

In order to meet the requirements for modern cast iron components, this multi-domain approach must employ methods from casting simulation, micromechanical analysis, topology optimization, and strength assessment. Here, casting simulation is used to determine local microstructure descriptors, which are subsequently used in micromechanical shakedown analysis to estimate the local microstructure-dependent fatigue strength. In parallel to the fatigue strength estimation, topology optimization is performed iteratively in combination with a castability analysis. The component strength is evaluated using a strength assessment approach based on the previously determined local material properties in combination with the topology optimized component.

In this study, the overall concept of the proposed multi-domain approach is presented and requirements for the application of such an approach are formulated. The use case of this study is a planet carrier of a wind turbine gearbox manufactured from austempered ductile cast iron ADI-GJS-1050-6. For this use case, a weight reduction of 17% was achieved while maintaining the required stiffness, such that the microstructure variance along the component was significantly reduced. Furthermore, the potentials and limitations of the presented approach are outlined and discussed in the context of the design of heavy-section castings.

Multi-Domain Optimierung von Gussbauteilen in Windenergieanlagen

Zusammenfassung

Im Zuge des Ausbaus der erneuerbaren Energien kommt es zu einem Zuwachs an Windenergieanlagen (WEA) mit gesteigerter Leistung. Durch Leistungsgewichte von bis zu 20 Tonnen Gusseisen je Megawatt in modernen WEA eröffnen sich neue Herausforderungen im Bereich des Bauteilgewichts, Fertigbarkeit und Gießbarkeit. Eine Lösung bieten systematische multi-domain Optimierungen, durch die das Bauteilgewicht reduziert sowie die lokale Auslastung des Bauteils gesteigert werden können.

✉ Felix Weber
f.weber@iwm.rwth-aachen.de

[1] Institute for Materials Applications in Mechanical Engineering, RWTH Aachen University, Augustinerbach 4, 52062 Aachen, Germany

[2] Chair for Wind Power Drives, RWTH Aachen University, Campus-Boulevard 61, 52074 Aachen, Germany

[3] Institute of Structural Mechanics and Lightweight Design, RWTH Aachen University, Wüllnerstraße 7, 52062 Aachen, Germany

[4] Access e. V., Intzestraße 5, 52072 Aachen, Germany

[5] MAGMA Gießereitechnologie GmbH, Kackertstraße 16–18, 52072 Aachen, Germany

[6] Silbitz Group Torgelow GmbH, Borkenstraße 15a, 17358 Torgelow, Germany

Um die Anforderungen an moderne Gussbauteile zu erfüllen, muss eine multi-domain Optimierung Methoden aus dem Feld der Gusssimulation, mikromechanischen Analyse, Topologieoptimierung und der Festigkeitsnachweise nutzen. Durch die Gusssimulation können Mikrostrukturdeskriptoren gewonnen werden, welche in der folgenden mikromechanischen Analyse zur Abschätzung mikrostrukturabhängiger Werkstoffeigenschaften verwendeten werden. Parallel dazu erfolgt eine iterative Topologieoptimierung unter kontinuierlicher Berücksichtigung der Gießbarkeit. Der Festigkeitsnachweis erfolgt auf Basis der bestimmten Werkstoffeigenschaften und der durchgeführten Topologieoptimierung.
In dieser Studie wird ein Konzept für eine multi-domain Optimierung vorgestellt und die Anforderungen für deren Anwendung dargestellt. Als Demonstrator dient ein aus ausferritischem Gusseisen der Güte ADI-GJS-1050-6 gefertigter Planetenträger. Für diesen Demonstrator konnten Gewichtseinsparungen von 17 % bei gleichbleibender Bauteilsteifigkeit erzielt werden. Darüber hinaus konnte die Mikrostrukturvariation innerhalb des Bauteils signifikant reduziert werden. Es erfolgt eine Bewertung des möglichen Potentials und möglicher Grenzen des vorgestellten Ansatzes im Kontext der Auslegung von dickwandigen Gussbauteilen.

1 Introduction

The transition towards a carbon-neutral society, the stated aim of the European Union [1], requires ambitious expansion targets for the installed renewable energy production. As wind turbines have become a cornerstone of renewable energy production, the expansion targets require an increase in installed wind turbine power. This can be achieved through an accelerated installation of wind turbines and an increase in wind turbine-specific power. However, modern wind turbines still contain up to 20 tons of cast iron per installed megawatt due to heavy-section castings such as torque arm, main shaft, or planet carrier that are subjected to cyclic loading during operation [2]. Thus, accelerated installation and up-scaling create challenges in manufacturing and logistics due to the component weight. The multi-domain lightweight design concepts enable the up-scaling of wind turbines to higher power density using weight-reduced components. The weight reduction in turn leads to an optimization of CO2 emissions over the entire life cycle of new wind turbines. Therefore, unused component potentials of heavy-section castings, such as those given by consideration of local material properties or new engineering materials, need to be exploited for component design process. This requires, firstly, the material properties to be numerically estimated based on limited microstructure information, and secondly, the local material properties to be considered in a component design concept.

For ductile cast iron, as used in wind turbines, microstructure-based modeling has been investigated using different approaches: Based on simplified unit-cell models, as used by Bonora et al. [3] to study damage mechanisms. More complex material models have been incorporated into advanced concepts, such as those used by Andriollo et al. [4, 5]. Utilizing the results of advanced material modeling, the behavior of ductile cast iron under cyclic loading has been investigated experimentally and numerically at the microscale [6–8]. Thereby, numerical approaches, such as the shakedown theorem, have been developed to determine the fatigue strength of a given microstructure [6, 9].

With respect to the consideration of local material properties in design concepts of cast iron components, Olofsson et al. [10, 11] have presented first multi-domain approaches. Here, local material properties are considered along a cast iron component based on the casting simulation results. Thus, a strength assessment of the component has been performed using the estimated local material properties [11, 12]. Progress has been made in other work in the field of topology optimization of castings. Li et al. took into account the manufacturing conditions in terms of gap dimensions and undercuts [13]. For this purpose, a quantity, virtual temperature, was defined, which allows specifying multidirectional demolding conditions. Approaches to stress-based topology optimization for castings were presented by Wang et al. [14]. Here, a comparison was made between a stress-based and a stiffness-based optimization. Recently, Lubenow et al. [15] used an optimization scheme of topology optimization, casting simulation, and local computer-aided optimization to optimize a planet carrier.

However, multi-domain design concepts with numerical fatigue strength estimation have not yet been applied to heavy-section castings made of austempered ductile cast iron, such as the planet carrier. For such components, the local microstructure varies significantly such that a numerical estimation of the local fatigue strength can reduce experimental requirements. In combination with the localized strength assessment a component potential can be opened up.

This study presents an approach to consider a local strength assessment in the design of heavy-section castings made of austempered ductile cast iron for wind turbines using a planet carrier as a demonstrator. Potentials for weight reduction under certain boundary conditions given by operating requirements are determined. The material investigated, an austempered ductile cast iron, is described for this use case. The fatigue strength is estimated using shakedown analysis of the microstructure. Combined with

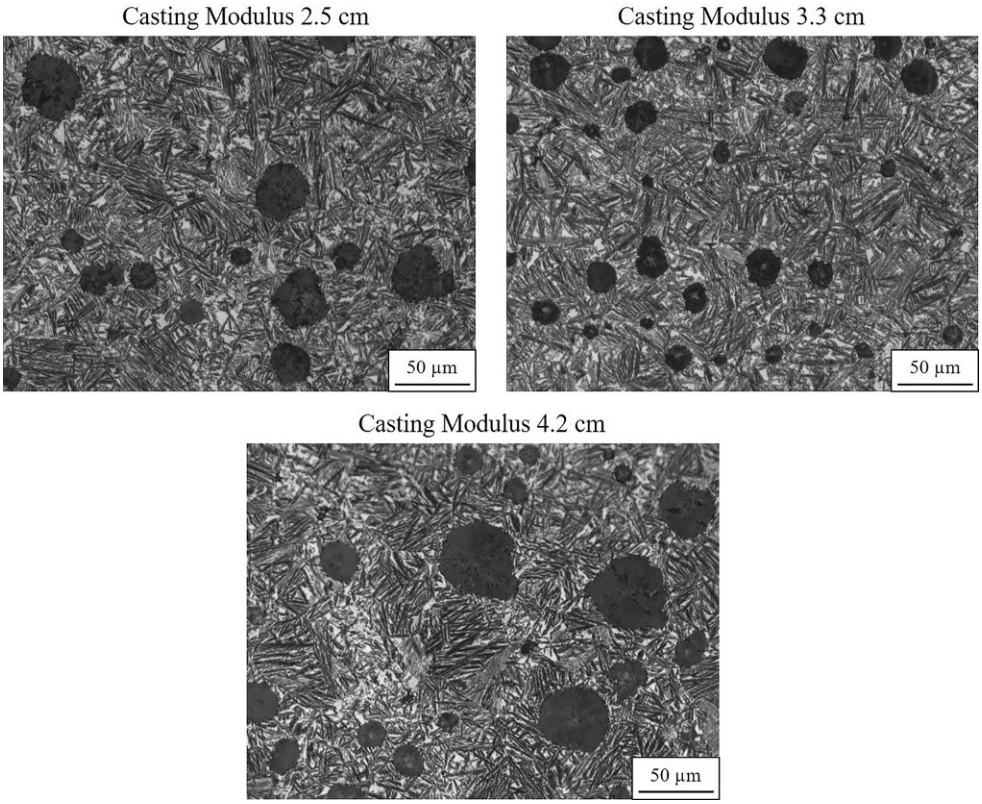

Fig. 1 Exemplary micrographs for casting modulus of 2.5, 3.3, and 4.2 cm

the casting simulation, this allows for a high resolution of local fatigue strength within the casting. Subsequently, topology optimization of the planet carrier is performed and a modified strength assessment is used to determine local utilization rates. Finally, the optimization potential of the planet carrier is estimated based on topology optimization and local strength assessment results.

Table 1 Analysis of microstructure descriptors according to EN 945-4

Casting Modulus	2.5 cm	3.3 cm	4.2 cm
Graphite Phase Fraction [%]	10.7	10.4	11.4
Max. Feret Diameter [µm]	21.46	20.59	26.15
Nodularity [%]	83.9	88.3	88.3
Particle Count [1/mm^2]	364	383	249

Table 2 Chemical analysis of the investigated austempered ductile cast iron grade ADI-GJS-1050-6

Element	wt.-%	Element	wt.-%
C	3.3	Mo	<0.33
Si	2	Mn	<0.3
Ni	1.99	Mg	<0.05
Cu	0.8	P	<0.03
Fe	Bal	–	–

2 Material

The material investigated in this study is a heavy-section cast of austempered ductile cast iron grade ADI-GJS-1050-6. Sampling was done using cubes of side lengths 150, 200, and 250 mm (casting modules 2.5, 3.3, and 4.2 cm, respectively) cast by Buchholz & Cie. foundry in a sand mold and heat treated by ADI treatments. The material was subjected to a two-stage heat treatment: austenitizing at 900 °C for 7 h and austempering at 300 °C for 4 h. Specimens were taken from the center of each cube for material characterization as well as fatigue testing. Exemplary micrographs are shown in Fig. 1 for each casting modulus. The microstructure descriptors analyzed according to standard EN 945-4 using five micrographs of size $1.387 \times 1.045\,\text{mm}^2$ at $100\times$ magnification are given in Table 1.

Chemical analysis was performed using a melt sample during casting with the results given in Table 2. Results of uniaxial tensile testing of five specimens of type A with

Table 3 Results of mechanical testing

Casting Modulus	2.5 cm	3.3 cm	4.5 cm
Ultimate Tensile Strength [MPa]	1003	934	839
Yield Strength [MPa]	736	683	640
Fracture Elongation [%]	9.27	9.25	6.31
1% Fatigue Strength (R = –1, uniaxial)	294	333	277

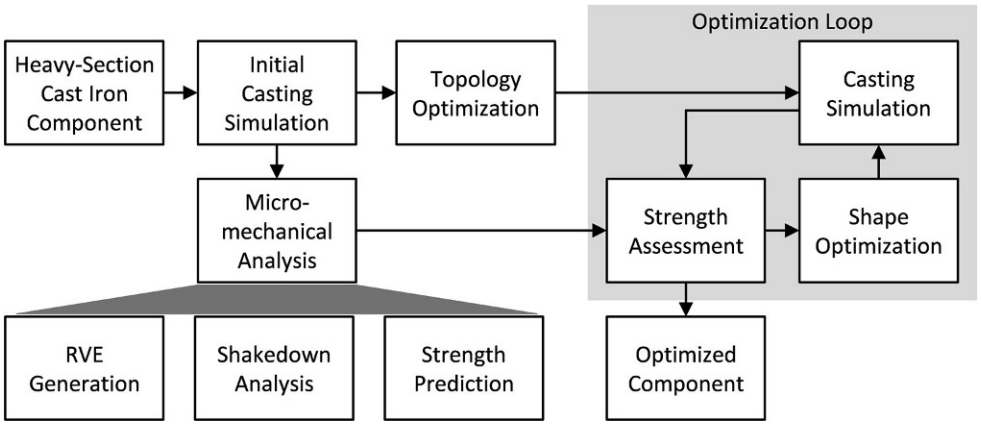

Fig. 2 Overview of the multi-domain optimization approach

a diameter of 10 mm according to DIN 50125 [16] are shown in Table 3. Additionally, results of fatigue testing (fatigue strength at a survival probability of 1%) according to DIN 50100 in a staircase testing procedure with a logarithmic increment of $d_{\log} = 1.069$ [17] are given in Table 3. Fatigue testing was performed on a Roell Amsler HFP 422. The remaining specimens and runouts were used to determine the finite life regime. The results were evaluated using the software SAFD 5 [18].

Comparing the experimentally determined fatigue strengths, a maximum can be observed at a casting modulus of 3.3 cm. This fits with the microstructure descriptors, as casting modulus 2.5 cm shows a reduced nodularity and casting modulus 4.2 cm an increased size of graphite precipitates. A possible reason for the increased fatigue strength at a casting modulus of 3.3 cm can be seen in the required alloying for a successful heat treatment, which depends on the wall thickness [19]. With 11.7% and 16.7% change in local fatigue strength, respectively, a significant influence of local microstructure and, thus, local solidification and heat treatment can be identified.

3 Methodology

3.1 Multi-domain optimization approach

The presented multi-domain optimization approach for cast iron components in wind turbines is characterized by the combination of casting simulation, topology optimization, micromechanical analysis, and strength assessment (see Fig. 2). Thus, it uses cross-scale simulation and allows an enhanced consideration of local material properties. Starting from an initial casting simulation, the microstructure of characteristic component regions is estimated and micromechanical analysis is performed for these regions. In parallel, a topology optimization in combination with castability analysis leads to a first optimized topology. In a subsequent optimization loop, the local material parameters, determined by micromechanical analysis, are considered in an iteration of strength assessment, shape optimization, and casting simulation.

3.2 Casting simulation

Within the presented approach, the casting simulation is used to estimate local solidification behavior and determine the castability of the optimized component. In contrast to the classical approach of solidification time prediction using the casting modulus, defined by the volume V and the cooling surface S, the thermal modulus (or feedmod) is used. Based on Chvorinov's rule [20] the casting modulus is proportional to the solidification time:

$$t_S = \mathrm{c} \cdot M^2$$

where c is a constant depending on cast alloy, mold material, and pouring temperature. Thus, the feedmod considers neighboring parts, auxiliary materials such as cooling chills, or transient heat flow conditions during cooling. Therefore, determining characteristic material regions in the investigated component under consideration of the feedmod allows an implicit consideration of solidification times.

3.3 Shakedown analysis

The micromechanical analysis, as a central element of the presented optimization approach, is based on the numerical determination of a shakedown state for a microstructure as a result of a casting simulation. A shakedown state can be reached under cyclic loading if, after initial loading cycles with plastic deformation, a purely elastic deformation occurs during loading. Weichert et al. [21] have investigated the shakedown state for composite materials. According to them, the shakedown state is governed by a time-invariant residual stress field $\overline{\rho}$, which is formed in the microstructure [21]. The residual stress field is caused by an accumulation of local plasticity and superimposes the purely elastic

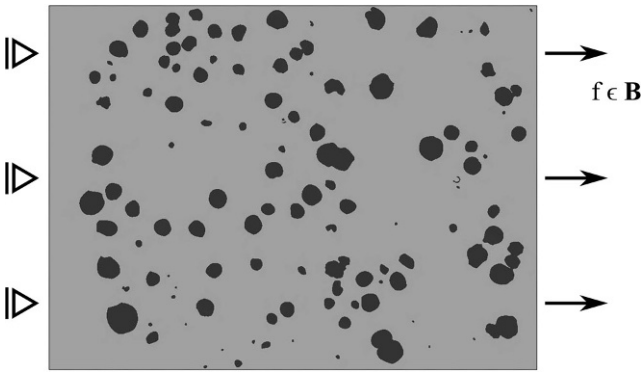

Fig. 3 Exemplary RVE with graphite precipitates (*dark*) and ferrite matrix (*gray*) and applied boundary conditions for shakedown analysis

stress field σ^e due to external loading [21]. The locally acting stress can be defined as:

$$\sigma = \sigma^e + \overline{\rho}$$

The plastic dissipation is bounded once a shakedown state, characterized by purely linear elastic loading, is reached. This prevents the formation of any further plastic strains in the microstructure [8].

Using Melan's static theorem for shakedown [22], the shakedown state can be determined:

> "If there exists a factor $\lambda > 1$ and a time-independent residual stress field $\overline{\rho}$ with
> $\int_{V'} \rho : \mathbb{D} : \rho dV < \infty$,
> with compliance tensor $\mathbb{D}$, such that for all loads **B** in the load domain the following inequality is satisfied
> $f(\lambda\sigma^e + \rho) \leq 0$,
> then the structure will shake down under the given load domain."

The FEM-based evaluation used in this study was implemented by Gebhardt [23], and yields the maximum admissible residual stress field under a given loading. Therefore, the following optimization problem, shown in non-discretized formulation, must be solved:

$$\begin{aligned} &\text{maximize} \quad \lambda \\ &\text{subject to} \quad \nabla \cdot \overline{\rho} \quad = 0 \text{ in } \Omega \\ &\qquad\qquad\quad \overline{\rho} \cdot n \quad = 0 \text{ on } \Gamma \\ &\mathrm{f}(\lambda\sigma_k^e + \overline{\rho}_k) \leq \sigma_Y^2 \quad \mathrm{k} = 1, .., \mathrm{NV} \end{aligned}$$

Table 4 Material parameters used in shakedown analysis

Material Property	Ausferrite Matrix	Graphite
Young's Modulus [GPa]	210	32
Poisson Ratio [–]	0.3	0.25
Yield Strength [MPa]	461.2	150

Here, *NV* represents the number of load vertices that define the load domain, Ω the computational domain, and Γ the boundary of the computational domain.

In order to apply the FEM-based evaluation an applicable computation domain representing the microstructure of interest must be supplied, typically in the form of a representative volume element (RVE). Here, RVE define a computational domain that is sufficiently large to represent the characteristics of the local cast iron microstructure. For a detailed description of the RVE construction, the reader is referred to [9]. An exemplary RVE of size $1.387 \times 1.045\,\mathrm{mm}^2$ is given in Fig. 3.

Material parameters of ausferrite and graphite used for shakedown analysis are summarized in Table 4. Graphite and ausferrite were considered to be linear elastic-ideally plastic. The yield strength of graphite is artificially increased to ensure the significance of the ausferrite matrix during shakedown. No debonding is considered at the interface of graphite precipitates and ferrite matrix.

3.4 Topology optimization

Topology optimization is used to determine the general component layout within the presented optimization approach. Therefore, following the initial casting simulation, an FE model of the component is created and split into modifiable design and non-modifiable non-design spaces. To ensure the maximum potential of the topology optimization, design spaces should fill as much available space as possible. Finally, the topology optimization can be formulated as minimization of an objective function *f* depending on a design variable *x*.

$$\min f(x)$$

Whereas the following restrictions must be met:

$$\begin{aligned} &g_j(x) \leq 0, j = 1, .., m_g \\ &h_k(x) = 0, k = 1, .., m_h \\ &x_i^l \leq x_i \leq x_i^u, j = 1...n \end{aligned}$$

Here, g_j are the inequality constraints, h_k are the equality constraints, and x_i^l and x_i^u are the upper and lower explicit constraints, respectively. However, functions have several local minima or maxima and it is not immediately evident whether the global maximum has already been found [24].

While different approaches exist, here the SIMP (Solid Isotropic Material with Penalization) approach is used for topology optimization. In solving the optimization problem, the density in an individual element of the FE-model is continuously varied between a minimum value ρ_{min} and the actual material density ρ^0. If the ratio of the local element

density ρ_e and the density of the material ρ^0 is formed, the relative density x_e is obtained as a design variable:

$$x_e = \frac{\rho_e}{\rho^0}$$

If x_e takes the value 1, solid material is present in the component at this point. If the value is less than 1, the local material stiffness in the form of the Young's modulus is reduced accordingly:

$$E_e = x_e^p E^0$$

Here, p is the so-called penalty exponent and E_e is the local material stiffness. It usually covers an interval between 2 and 4 [25].

3.5 Strength assessment

The strength assessment of the cast iron components to be optimized in presented approach is based on the international standard IEC 61400 (IEC 61400-4 for wind turbine gearboxes) [26]. This specifies the essential design requirements for ensuring the structural integrity of wind turbines and their components. One requirement is that the strength assessment must be based on validated and recognized methods which consider, for example, the size effect on material strength.

The strength assessment in this optimization approach is performed according to the FKM guideline. The process of strength assessment according to FKM follows a defined procedure for determining material parameters and component design parameters up to the degree of utilization [27]. In this work, the process was automated and extended to include local material parameters.

4 Results and discussion

The concept of the presented optimization approach is demonstrated using a planet carrier made of ADI-GJS-1050-6. Therefore, first an initial topology optimization was performed and subsequently its effect on the local microstructure was analyzed. Finally, the effects of local fatigue strength on the utilization were analyzed.

4.1 Topology optimization of planet carrier

In order to show the maximum possible optimization potential, the initial geometry was reworked prior to topology optimization. This geometry extension is to ensure that the maximum possible weight reduction is achieved during topology optimization. Figure 4a shows a sectional view of the planet carrier. Here, the yellow part indicates the initial geometry and the magenta part the volume extension for topology optimization. The outer diameter of the planet carrier was slightly enlarged compared to the initial geometry. Furthermore, the inside diameter was reduced to the diameter of the tip of the sun gear.

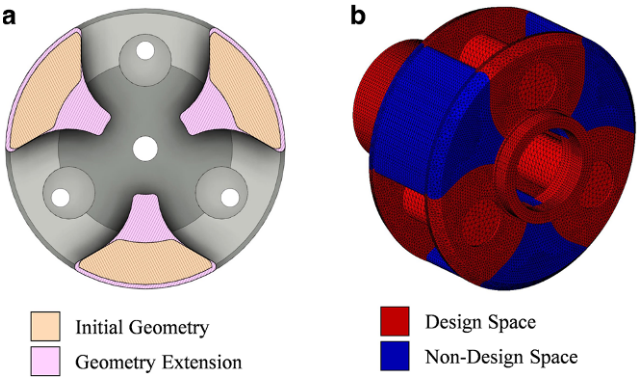

Fig. 4 Extension of the planet carrier's volume (**a**) and definition of design- and non-design space (**b**)

The design space available for topology optimization is visualized as blue regions in Fig. 4b. It is limited by the optimization restriction of constant local stiffness at the mounting for the planetary gears. The red area shows the non-design space, i.e. the part that remains unchanged after the topology optimization. Due to the increased design space, the mass of the planet carrier increases by 22%.

Boundary conditions and loadings considered during the topology optimization as well as for the determination of stresses for the strength assessment are visualized in Fig. 5. Here, all degrees of freedom of the coupling surface were fixed. The maximum torsional load from the power production on normal turbulence design load case (DLC) 1.2 [28] was applied via circumferential forces acting on the planetary gear pins. The bearing surfaces of the planet carrier were only fixed in the radial direction. The topology optimization was carried out using constant material properties

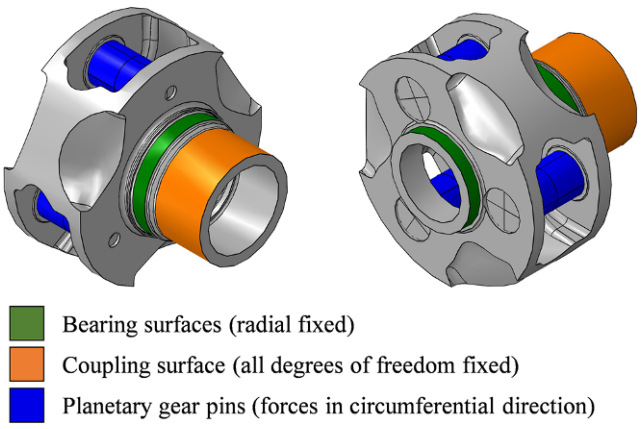

Fig. 5 Boundary conditions of the FE model of the planet carrier

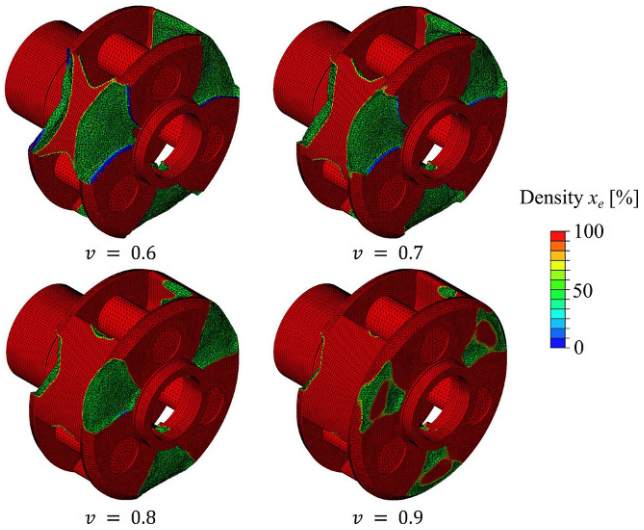

Fig. 6 Results of the topology optimization for different target volumes (elements with a resulting density x_e below 50% are removed for visualization)

for the entire planet carrier, such as Young's modulus of 168 GPa and a Poisson's ratio of 0.27.

Concerning system stability, weight reduction was facilitated under the boundary condition of constant stiffness during power production load case DLC 1.2 and castability. The system stability requirement is intended to ensure that the system behavior remains unchanged after optimization for the power production load case. In this context, system stability was determined by evaluating allowable deformation and component stiffness. Therefore, seven different optimizations with different target volumes were carried out to determine the resulting change in torsional stiffness of the planet carrier for a given change in weight compared to

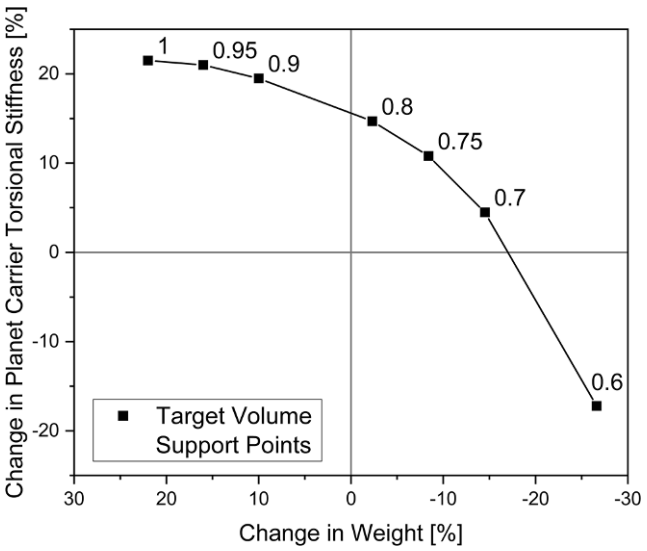

Fig. 7 Change in torsional stiffness vs. change in weight of the planet carrier compared to the initial geometry for torsional loading

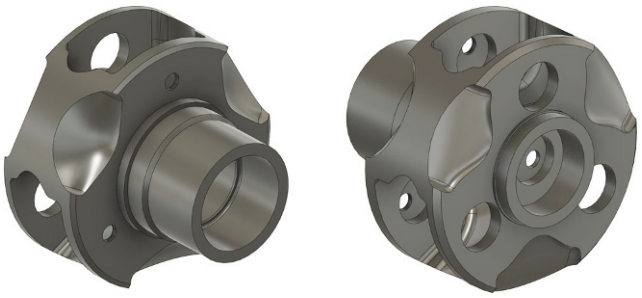

Fig. 8 Result of the topology optimization of the planet carrier

the initial geometry. Target volume v_i specifies how much of the extended geometry volume remains after optimization. Figure 6 illustrates some results of topology optimization for different target volumes.

Figure 7 depicts the relation between the change in torsional stiffness and weight of the planet carrier compared to the initial geometry for different target volumes. Positive values imply an improvement in torsional stiffness and an increase in the weight of the planet carrier. It can be seen that the torsional stiffness of the planet carrier can be maintained despite a reduction in mass. Moreover, compared to the initial geometry, an increase in torsional stiffness of about 16% can be achieved with the same mass. If the torsional stiffness is kept constant, a weight reduction of about 17% is achieved.

According to Fig. 7, a target volume of slightly less than 70% provides a torsional stiffness similar to the initial planet carrier design. For this reason, this geometry resulting from the topology optimization is chosen as the basis for the new design. In order to exploit the highest weight-saving potential, the planet carrier is reconstructed as close as possible to the optimized geometry. The first design of the planet carrier can be seen in Fig. 8. Compared to the initial geometry, a weight reduction of 17.6% is achieved.

As shown in Fig. 8, pockets were formed at the front and rear of the planet carrier, which protruded into the body. In top view, an x-shape structure results, caused by the fact that the planet carrier is predominantly subjected to torsion, so that mainly shear stresses have to be transmitted. Since the main stress direction is rotated by about 45° to the center axis, diagonal structures are formed. The structure described is smaller on the gearbox side, since a large proportion of the load is already distributed over the planetary gear pins. Noticeably, the pocket extends to the bearing seat and even forms a small opening. Comparing the influence of the target volume, only the intensity of the described characteristics varies.

Figure 9 shows the deformation within the planet carrier and the planetary gear pins under the same loading for the initial planet carrier geometry and the 17.6% weight-reduced planet carrier with the same torsional stiffness. As

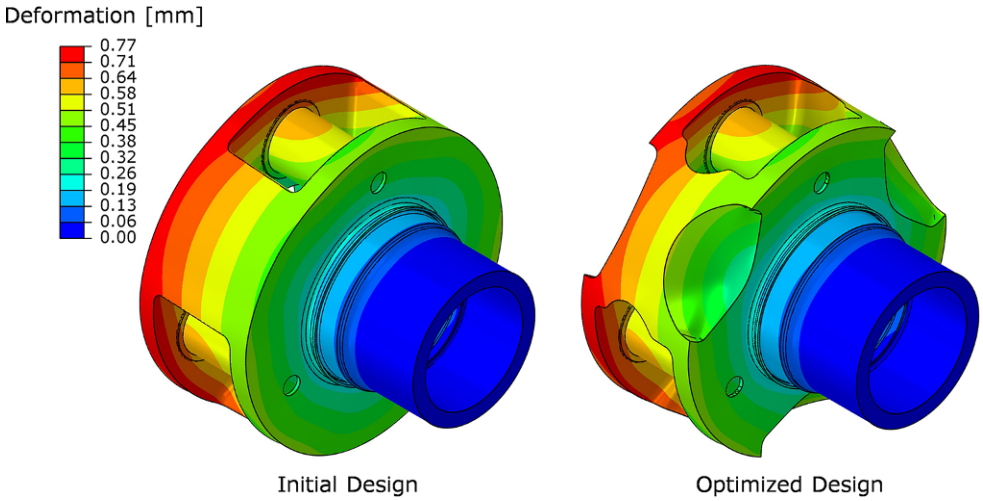

Fig. 9 Comparison of the deformations of initial planet carrier design and optimized design (weight reduction 17.6%)

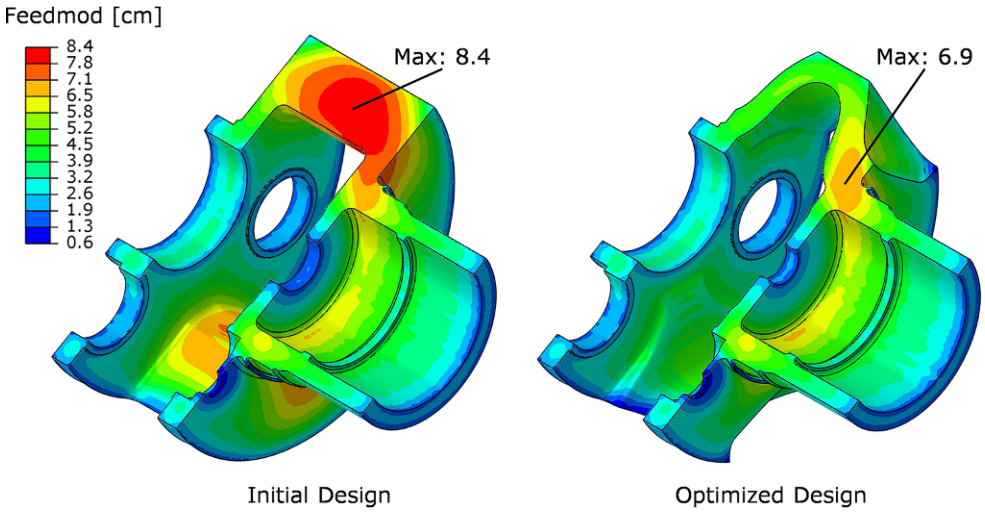

Fig. 10 Feedmod distribution in the initial design and the optimized design

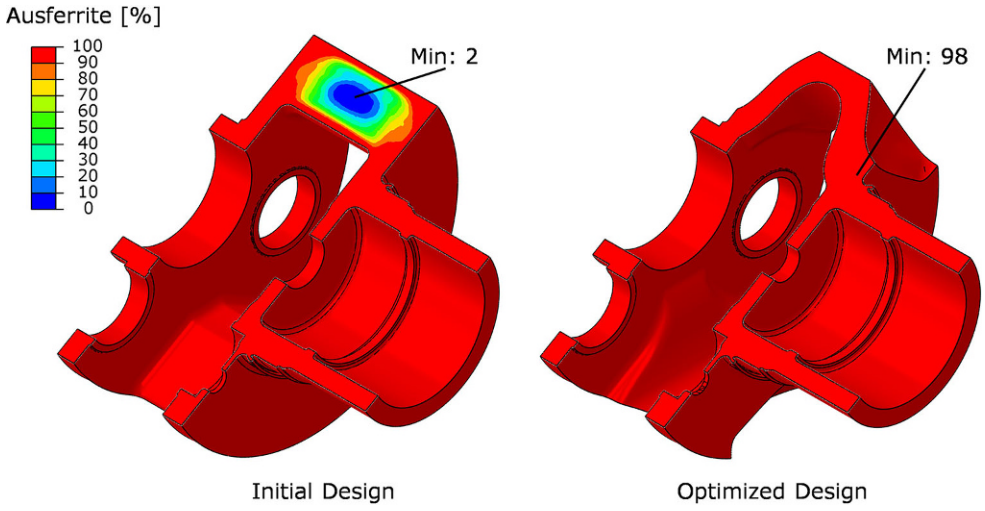

Fig. 11 Expected ausferrite distribution in the initial and optimized component design

indicated by the constant stiffness, no significant difference in local deformation can be observed. However, these values represent theoretical optimum values that may not be achieved in practice due to manufacturing-related design changes or cost considerations.

4.2 Analysis of topology optimized planet carrier with respect to manufacturability

As the planet carrier is made out of ADI-GJS-1050-6, component optimization must also consider the characteristics of the manufacturing route, e.g. heat treatment, besides the overall goal of weight reduction while maintaining system stability. Concerning the manufacturing route, the local distribution of feedmods and efficiency of the heat treatment were analyzed.

Since manufacturing of ADI depends on both initial raw material and heat treatment, the melt is adjusted to reliably set ADI microstructure in the critical component regions. Thus, to evaluate the component optimization with respect to the working material, the feedmod distribution and the phase fraction of ausferrite after heat treatment were analyzed.

Figure 10 shows that the scatter of feedmods can be significantly reduced by reducing the maximum feedmod from 8.4 to 6.9 cm. A reduction of the feedmod range allows a better adjustment of the melt, especially regarding hardening agents and other alloying elements. The minimum of non-transformed austenite (after quenching), as shown in Fig. 11, increases from 2 to 98%. Thus, large non-ausferrite regions could be eliminated and a more successful ausferritization can be expected.

4.3 Strength assessment with local fatigue strength

Considering the complex adjustments required for successful ADI manufacturing, the importance of local material properties increases as local effects in the planet carrier must be considered. To account for local material properties, experimentally determined local ultimate tensile strength and simulated local shakedown limits (used as fatigue strength) were considered in strength assessment. Here, the shakedown limits were computed using 15 RVE of size $500 \times 500 \times 20\,\mu m^3$ per feedmod. Due to computational cost, the fatigue strength was computed for support points of the feedmod within the critical regions of the torque arm, resulting in feedmods within the range of 2.5–4.2 cm.

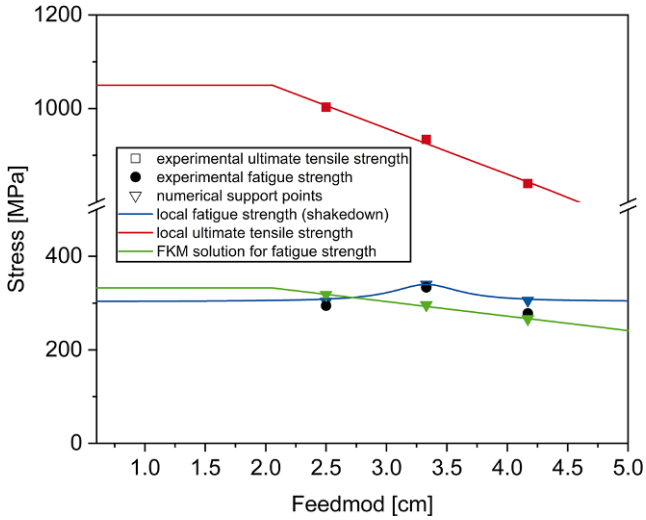

Fig. 12 Functions of ultimate tensile strength and fatigue strength used during strength assessment

The strength curves as a function of feedmod are shown in Fig. 12. Here, the non-linearity of the fatigue strength with respect to the feedmod can be observed. This non-linearity may be associated with the interdependence of graphite precipitates and ausferrite matrix. This may be related to the ADI manufacturing, which is governed by a heat treatment process window and special requirements regard-

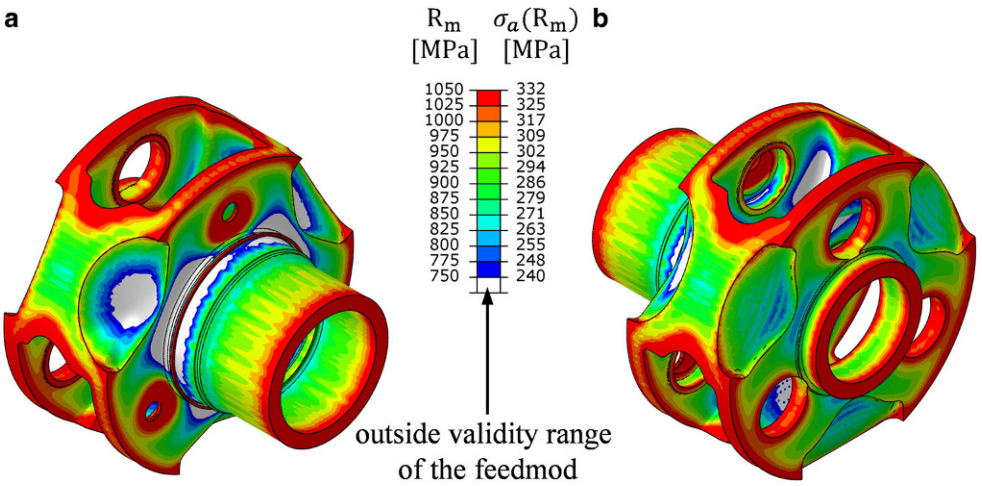

Fig. 13 Local ultimate tensile strength (**a**) and estimated FKM—fatigue strength (**b**)

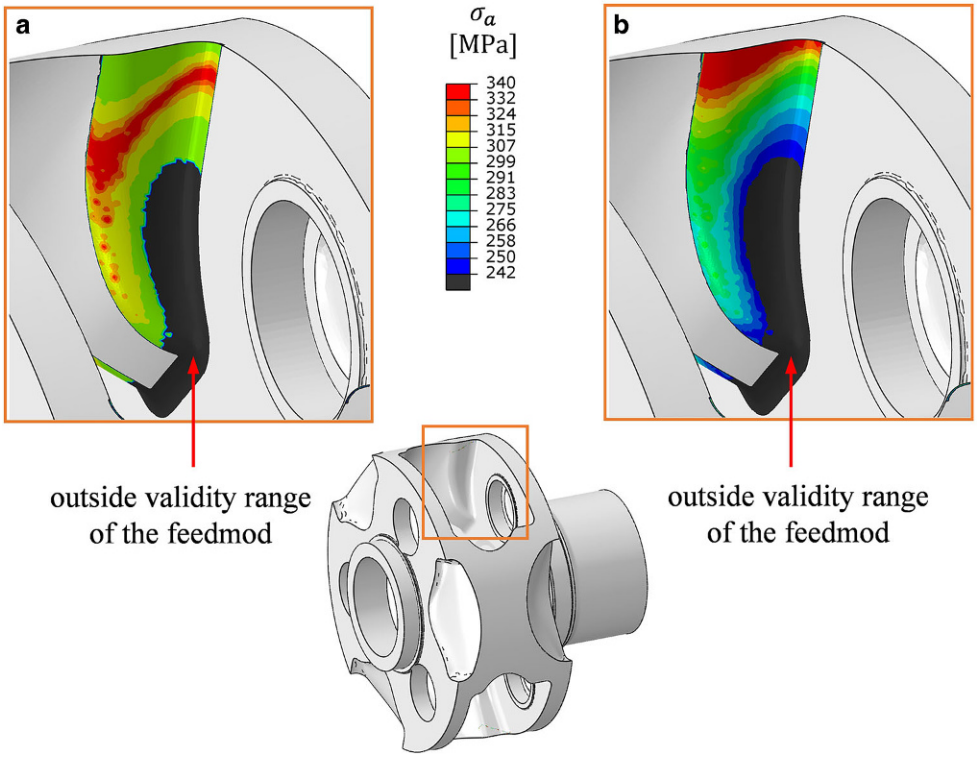

Fig. 14 Local fatigue strength obtained by shakedown analysis (**a**) compared to the FKM—fatigue strength (**b**)

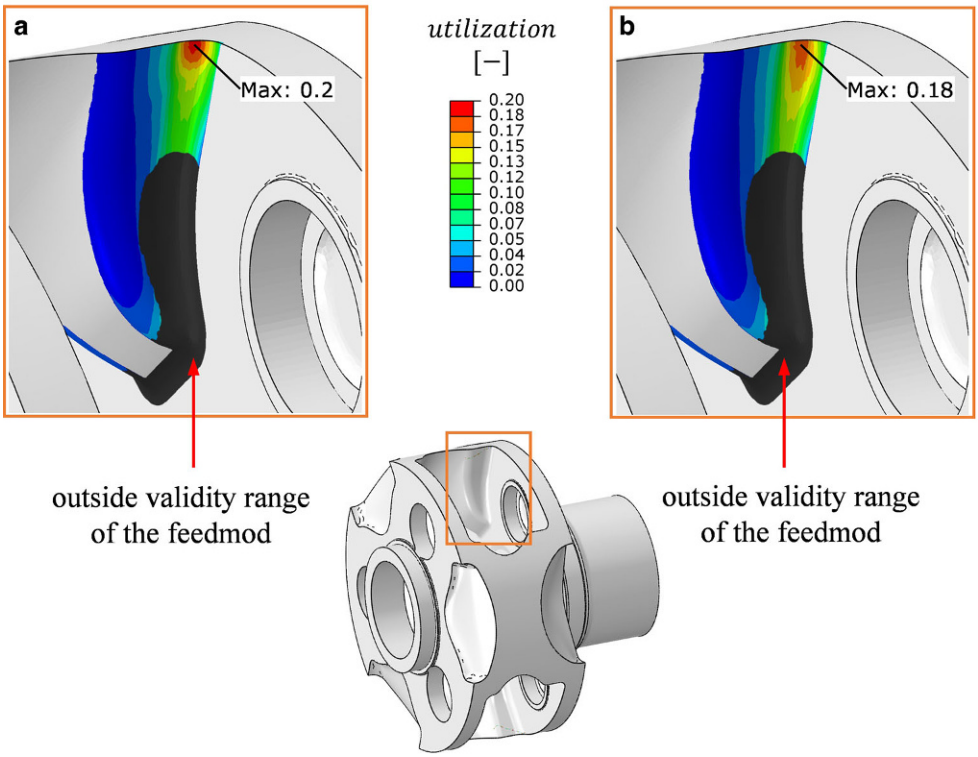

Fig. 15 Local fatigue strength utilization using the results of shakedown analysis (**a**) and FKM—fatigue strength (**b**)

ing alloying of wall-thickness dependent elements [19]. Thus, optimal material parameters for the given use case may only be present at a specific feedmod, whereas lower feedmods may have passed the ideal process window while higher feedmods have not have reached the ideal process window. Due to limited experimental validation, the maximum feedmod of 5 cm was set as the bound of the validity range.

The locally resolved ultimate tensile strength as a function of the feedmod and the fatigue strength estimated using this ultimate tensile strength are shown in Fig. 13. The conversion of ultimate tensile strength into a fatigue strength (hereinafter referred to as FKM—fatigue strength) was carried out following the FKM guideline [27]:

$$\sigma_a\,(R_m) = (0.25 + \frac{70MPa}{1050MPa}) \cdot R_m(feedmod)$$

Highest ultimate tensile strength and fatigue strength can be observed in regions with lowest feedmods, e.g. close to the surface of the component and at the corners. However, this relation does not account for the observed non-linearity of fatigue strength with respect to the feedmod.

In Fig. 14, the locally resolved FKM—fatigue strength and fatigue strength according to shakedown analysis are compared within the critical notch. It can be seen that the regions of the highest fatigue strength can be found at a given offset from the surface of the component if fatigue strengths based on shakedown analysis are considered. Especially close to the surface a difference of 15% between FKM—fatigue strength and fatigue strength based on shakedown analysis can be observed.

The local utilization is shown in Fig. 15. For both cases, FKM—fatigue strength and fatigue strength based on shakedown analysis, the local utilization rates remain below 20%. This is related to the optimization requirements of the planet carrier, so local fatigue damage can be neglected for the given combination of considered loads and material. However, if the local utilization increases, the local fatigue strength within a component of austempered ductile cast iron becomes significantly more relevant.

5 Conclusion and outlook

This study demonstrates the consideration of local material properties in component design of heavy-section castings used in wind turbines. An improved understanding of the consideration of local material properties, especially for complex material systems such as austempered ductile cast iron, was achieved. Subsequent component optimization, resulted in significant weight reduction under the overall constraints of castability and system stability.

Heavy-section castings of austempered ductile iron grade ADI-GJS-1050-6 were characterized. Results of material characterization were used as calibration parameters for the presented multi-domain optimization approach, which was demonstrated using a planet carrier. Thereby, casting simulations have been used to compute local microstructure characteristics in critical regions of the planet carrier. For a set of supporting points of these microstructure characteristics, the shakedown analysis was used to numerically determine microstructure-dependent fatigue strengths. In parallel, a topology optimization of the planet carrier was performed and a significant weight reduction potential of 17% was identified while maintaining the required initial component stiffness. The effect of topology optimization on local material quality was determined by comparing feedmod scattering and expected local ausferrite phase fraction. Here, the topology optimization resulted in an improvement of both feedmod scattering and local ferrite phase fraction. Thus, it was shown that topology optimization reduces component weight and can increase the local material quality within the component for austempered ductile iron.

The local utilization was computed using fatigue strength estimates based on the ultimate tensile strength and fatigue strength obtained by shakedown analysis. Here, good agreement between both with a difference of 15% could be observed. It was shown that analysis of local fatigue strengths allows the derivation of required changes in manufacturing, e.g. the adjustment of the heat treatment process to achieve the highest fatigue strengths close to the surface. Overall, the presented multi-domain optimization approach resulted in an optimized planet carrier with a weight reduction of 17% while maintaining the required stiffness and reduced microstructure variance along the component. Due to the high strength of the used material ADI-GJS-1050-6, the strength assessment was neglectable compared to the required stiffness for the optimized planet carrier. Thus, the strength assessment was irrelevant to the demonstrated weight reduction. Nevertheless, this method can be applied to other heavy-section castings where consideration of local material properties during strength assessment may be advantageous for the component design.

Future work will continue to integrate local material properties into strength assessment concepts of heavy-section castings used in wind turbines. The applicability of the approach needs to be validated by investigating other geometries and other austempered ductile cast iron grades. The estimation of local fatigue strength using the shakedown approach will be extended to include a criterion to account for local permissible damage. To reduce safety factors in the future, the interaction of safety factors with local material properties and local material quality will be determined.

Funding This research has been funded by the Federal Ministry for Economic Affairs and Climate Action (BMWK) in the project LeKo-Guss WEA under grant number 0324279A. The authors acknowledge the support by Siemens PLM, agreement 60068580, for providing STAR-CCM+ licenses.

Supported by:

on the basis of a decision
by the German Bundestag

Funding Open Access funding enabled and organized by Projekt DEAL.

References

1. European Commission (2018) The Commission calls for a climate neutral Europe by 2050
2. Bundesverband der Deutschen Gießerei-Industrie (2016) Die Gießerei-Industrie
3. Bonora N, Ruggiero A (2005) Micromechanical modeling of ductile cast iron incorporating damage. Part I: Ferritic ductile cast iron. Int J Solids Struct 42:1401–1424
4. Andriollo T, Thorborg J, Hattel J (2016) Modeling the elastic behavior of ductile cast iron including anisotropy in the graphite nodules. Int J Solids Struct 100–101:523–535
5. Andriollo T, Thorborg J, Tiedje NS, Hattel J (2015) Modeling of damage in ductile cast iron—the effect of including plasticity in the graphite nodules. IOP Conf Ser Mater Sci Eng 84:12027
6. Gebhardt C, Chen G, Bezold A, Broeckmann C (2018) Influence of graphite morphology on static and cyclic strength of ferritic nodular cast iron. MATEC Web Conf 165:14014
7. Gebhardt C, Sedlatschek T, Bezold A, Broeckmann C (2021) Full-field inverse identification of elasto-plastic model parameters for ductile cast iron. Mech Mater 162:104056
8. Chen G (2016) Strength prediction of particulate reinforced metal matrix composites. Shaker, Aachen
9. Gebhardt C, Trimborn T, Weber F, Bezold A, Broeckmann C, Herty M (2020) Simplified ResNet approach for data driven prediction of microstructure-fatigue relationship. Mech Mater 151:103625
10. Olofsson J, Salomonsson K, Svensson IL (2015) Modelling and simulations of ductile iron solidification—induced variations in mechanical behaviour on component and microstructural level. IOP Conf Ser Mater Sci Eng 84:12026
11. Olofsson J, Salomonsson K, Johansson J, Amouzgar K (2017) A methodology for microstructure-based structural optimization of cast and injection moulded parts using knowledge-based design automation. Adv Eng Softw 109:44–52
12. Olofsson J, Cenni R, Cova M, Bertuzzi G, Salomonsson K, Johansson J (2018) Multidisciplinary shape optimization of ductile iron castings by considering local microstructure and material behaviour. Struct Multidisc Optim 57:1889–1903
13. Li Q, Chen W, Liu S, Fan H (2018) Topology optimization design of cast parts based on virtual temperature method. Comput Aided Des 94:28–40
14. Wang C, Xu B, Duan Z, Rong J (2021) Stress-related topology optimization for castable design. Numerical Meth Engineering 122:6203–6233
15. Lubenow K, Schuhmann F, Schemmert S (2019) In: Proc. Conf. for Wind Power Drives Aachen (CWD2019)
16. DIN German Institute for Standardization, Testing of metallic materials: Tensile test pieces 77.040.10(50125), Berlin, Beuth Verlag GmbH, 2022.
17. DIN German Institute for Standardization, Load controlled fatigue testing: Execution and evaluation of cyclic tests at constant load amplitudes on metallic specimens and components 19.060(50100), 2016.
18. Hempen M, Klubberg F, Beiss P (1998) PC-Software SAFD—statistical analysis of fatigue data
19. Olawale JO, Oluwasegun KM (2016) Austempered ductile iron (ADI): a review. Matls Perf Charact 5:20160053
20. Jelínek P, Elbel T (2010) Chvorinov's rule and determination of coefficient of heat accumulation of moulds with non-quartz base sands. Arch Foundry Eng 10:77–82
21. Weichert D, Hachemi A, Schwabe F (1999) Shakedown analysis of composites. Mech Res Commun 26:309–318
22. Melan E (1938) Zur Plastizität des räumlichen Kontinuums. Ingenieur Arch 9:116–126
23. Gebhardt NC (2022) Einfluss der Graphitmorphologie auf die Langzeitfestigkeit von Gusseisen mit Kugelgraphit, 1st edn. Shaker, Düren
24. Schumacher A (2020) Optimierung mechanischer Strukturen. Springer, Berlin, Heidelberg
25. Bendsøe MP, Bendsøe MP, Sigmund O (2003) Topology optimization: theory, methods and applications. Springer, Berlin, Heidelberg
26. DIN German Institute for Standardization, Wind energy generation systems: Part 4: Design requirements for wind turbine gearboxes, 61400th ed. 27.180(61400-4), 2012.
27. Rennert R, Kullig E, Vormwald M (2020) Analytical strength assessment of components made of steel, cast iron and Aluminium materials in mechanical engineering: FKM guideline, 7th edn. VDMA, Frankfurt/Main
28. DIN German Institute for Standardization, Wind energy generation systems: Part 1: Design requirements, 61400th ed. 27.180(61400-1), 2012.